Journal of Power Sources 195 (2010) 6434–6442

Contents lists available at ScienceDirect

Journal of Power Sources

journal homepage: www.elsevier.com/locate/jpowsour

Inorganic–organic hybrid polymer electrolyte based on polysiloxane/poly(maleic imide-*co*-styrene) network

P.-L. Kuo[a,*], W.-H. Jheng[a], W.-J. Liang[b], W.-F. Chen[a]

[a] *Department of Chemical Engineering, National Cheng Kung University, Tainan City 70101, Taiwan*
[b] *Fire Protection and Safety Research Center, National Cheng Kung University, Tainan City, Taiwan*

ARTICLE INFO

Article history:
Received 9 February 2010
Received in revised form 17 March 2010
Accepted 24 March 2010
Available online 31 March 2010

Keywords:
Composites
Cross-linking
Polysiloxanes
Ionomers
Thin films

ABSTRACT

Covalently cross-linked nonfluorinated hydrocarbon ionomers are synthesized by introducing sulfonate groups and a siloxane cross-linker through thermally and chemically stable imide bonding on poly(styrene-*co*-maleic anhydride). The three-dimensional polysiloxane framework, which does not only act as a robust scaffold but also provide sites for the hydrogen bonding with water, contribute to the increase in bound water degree, higher proton conductivity at lower ion exchange capacity, and greatly decreased methanol permeability. The spherical-shaped ionic clusters produce a comparable proton conductivity (10^{-1} S cm^{-1} above 60 °C) to Nafion-117. The conductivity of the hybrid ionomer does not decrease to gain its selectivity, but instead increased. Methanol permeability is ~70% lower than that of Nafion-117, but has a higher water uptake and IEC. The membrane with IEC values of 1.1 mequiv. g^{-1} exhibits a constant conductivity for 200 h in hydrolytic stability test, and produce a power density 20% higher than Nafion-117 in single DMFC operation.

1. Introduction

Fuel cells are clean and efficient electrochemical power source that generate electric power via chemical reaction of fuels and oxygen and therefore have received a great deal of attention as potential high energy density power supplies [1–4]. Perfluorinated ionomers (Nafion®, du Pont) has long been the standard polymer for use in proton exchange membrane fuel cells (PEMFCs) and direct methanol fuel cells (DMFCs) [5,6]. The main purpose for the electrolyte is to allow protons to pass through freely while being a barrier to electrons and reactants. The perfluorinated ionomers are highly proton conductive upon hydration with water and chemically and physically stable at a temperature lower than 100 °C, however, fail as a barrier to methanol solutions. High methanol permeability, high cost, and environmental concerns of the fluorinated materials are also serious drawbacks for the practical application of this type of fuel cell applications [7].

Alternatively, there has been interest in developing nonfluorinated ionomers having the capacity to conduct protons. Engineering thermal plastics, acid-doped polymers, and solid acids with superprotonic phase transitions all fall within this category [8–10]. As has been recently reviewed, interest in such materials has led to the development of blending nonfluorinated ionomers with inorganic fillers, such as SiO_2 and nanoclay, as well as inorganic acids and superprotonic oxides [11]. The blending technique, which is appearing to be an extremely promising chemical modification approach, is capable of combining the desirable features of each blend component, while simultaneously reducing their drawbacks [12,13]. However, a major research aim is to incorporate extrinsic species into ionomers in stable structures while maintaining high proton conductivity. Cross-linking is a simple and efficient way to retain the indispensable properties of controllable swelling degrees, high proton conductivity, and dimensional stability [9]. Another key issue which should be addressed for the practical use of DMFCs is fuel permeation, which can be controlled effectively by means of adjusting the cross-linking density of the ionomers. In addition, the cross-linking technique's cost-effectiveness distinguishes it from the existing techniques. Film forming polymers with organic-based segments such as aniline [14] and imidazole [15] have been incorporated with sulfonated ionomers for the preparation of ionic cross-linking acid–base blend membranes. Covalent cross-linking has been achieved for sulfonated polyimides [16], poly(etheretherketone) [17], polysulfone [18], and polybenzimidazole [19] without sacrificing too much proton conductivity.

Through the tailoring of hybrid organic–inorganic composites at the molecular level, we have developed a series of ionic conducting polymers with fast lithium ion conduction and proton conduction [20–23]. One of our most important findings is that the introduction of a cross-linked polysiloxane framework into the matrix may help organic polymer electrolytes coalesce with inorganic silica nodes,

* Corresponding author. Tel.: +886 6 275 7575x62658; fax: +886 6 276 2331.
E-mail address: plkuo@mail.ncku.edu.tw (P.-L. Kuo).

0378-7753/$ – see front matter © 2010 Elsevier B.V. All rights reserved.
doi:10.1016/j.jpowsour.2010.03.068

and retain essential properties such as dimensional stability, high proton conductivity, and low methanol permeation [24,25].

In this paper, we synthesized a new type of covalently cross-linked hydrocarbon ionomer by introducing sulfonate groups and a siloxane cross-linker through thermally and chemically stable imide bonding. The polysiloxane framework, in addition to acting as a robust scaffold, provides sites for hydrogen–water bonding. The sulfonate and hydroxyl groups and the silica nodes allow the formation of a bound water layer that facilitates the conduction of protons, but obstructs the permeation of methanol fuel. Detailed investigation on the properties of these hybrid ionomers is reported. The proton conductivity, microphase structure, methanol permeability, and thermal and hydrolytic behaviors are described and compared to those of the Nafion membrane. DMFC operation with the hybrid ionomer is also demonstrated.

2. Experimental

2.1. Materials

Poly(styrene-*co*-maleic anhydride) (SMA, styrene:maleic anhydride = 1:1, molecule weight: 350,000) was purchased from Elf Atochem. Dimethyl sulfoxide (DMSO, Tedia) was freshly distilled from calcium hydride before use. 2-Aminoethanesulfonic acid and sodium hydroxide (NaOH) were obtained from Sigma. Aminopropyltriethoxysilane (APTES) was supplied by Dow Corning Corporation. Hydrochloric acid (37%) was from Riedel-de Haën. Nafion®-117 membrane was supplied from DuPont Fluoroproducts. Other chemicals including nitric acid (HNO_3, 69.5 wt.%), sodium chloride (NaCl), methanol (CH_3OH), sulfuric acid (H_2SO_4) were obtained from Aldrich. All aqueous solutions were prepared using deionized water purified through a Milli-Q system.

2.2. Membrane preparation

The synthesis of polysiloxane cross-linked sulfonated poly(maleic imide-co-styrene) is shown in Scheme 1. Sodium aminoethanesulfonate (AESA-Na) was obtained by mixing aminoethanesulfonic acid (AESA) with equal molar NaOH in water at 60 °C for 1 day. A typical procedure for preparing the membrane is as follows. 1.5 g of SMA (7.4×10^{-3} equiv. of anhydride) was dissolved in 30 ml of dry DMSO in a three-necked flask at 80 °C equipped with N_2 inlet. AESA-Na (2.5 mmol) also being dissolved in DMSO was dropped and mixed well. The temperature was kept at 80 °C. After 3 h, APTES (5.1 mmol) in DMSO was dropped slowly into the mixture and vigorously stirred at 80 °C for another 3 h. Subsequently, 16.8 mmol of water was added and stirred for 1 h. The solution was then cooled to room temperature and concentrated by using a rotary evaporator. The viscous mixture was poured onto an aluminum plate, and followed by slowly removing the residual solvent at 80 °C for 6 h and 120 °C for 2 h. After thermal imidization at 200 °C under vacuum for 48 h, brownish and transparent crude membranes with a thickness in the range of 150–200 μm in sodium salt form were obtained. The films were immersed in 1N HCl aqueous solution for 2 days and soaked in deionized water for 1 day so as to obtain H^+-form membranes. The water washing process was repeated 3 times. The membranes with different IEC was prepared by changing the molar ratio of AESA-Na and APTES (the repeat unit of AESA-Na, $x = 0.077$, 0.199, 0.234, 0.313 for membranes **A**, **B**, **C**, **D**, respectively).

2.3. Characterization

FT-IR spectra were recorded on a Nicolet 5700 system in the range of 4000–450 cm^{-1}. Each sample was prepared by mixing with potassium bromide (KBr) pellet and vacuum-dried at 80 °C to remove adsorbed water in the sample.

High-resolution solid-state NMR experiments were carried out on a Bruker AVANCE 400 spectrometer, equipped with a 7 mm double-resonance probe. The Larmor frequencies for ^1H, ^{13}C and ^{29}Si nuclei are 400.17, 100.58 and 79.46 MHz, respectively. Magic angle spinning (MAS) of the samples in the range of 5 kHz was employed for obtaining NMR spectra. The Hartmann–Hahn condition for $^1H \rightarrow {}^{13}C$ cross-polarization (CP) experiments was determined using adamantane, and proton decoupling was applied during acquisition to enhance the spectra sensitivity. Typically, a repetition time of 5 s was used in all the NMR experiments. The ^{29}Si, ^{13}C and ^1H chemical shifts were externally referenced to tetramethylsilane (TMS) at 0.0 ppm. A proton decoupling field strength of 60 kHz was used in all experiments.

The ion exchange capacity (IEC) was measured by classical titration. The membrane was soaked in a saturated NaCl solution. Released protons were titrated using 0.05N NaOH aqueous solution.

The tensile properties of specimens were determined using Instron tensile testing machine equipped with an extensometer. Dumbbell-shaped specimens with a gauge length and a width of 10 and 4 mm, respectively, were stretched with a strain rate of 8.3×10^{-3} s^{-1} at room temperature. Breaking stress was determined from the stress–strain curve.

Differential scanning calorimetry (DSC) measurement for dry membranes was conducted on a Du Pont TA2010 analyzer over the temperature range of 50–200 °C at a heating rate of 20 °C min^{-1} under dry nitrogen atmosphere. An empty aluminum pan was used as a reference. Two types of water, freezing and nonfreezing water (bound water), in the fully hydrated membranes were detected by melting transitions between −50 and +40 °C. The samples were first cooled from +25 to −50 °C, and then heated at a rate of 5 °C min^{-1} up to +40 °C. Calculation of the amount of free water (ω_f) in the samples was done by integrating transition heat capacity (ΔC_P) over the broad melting temperature interval in

$$\omega_f = \frac{\Delta H_m}{Q_{melting}} = \frac{\int \Delta C_P dT}{Q_{melting}}$$

where $Q_{melting}$ is the heat of fusion of bulk ice (334 J g^{-1}). The weight fraction of bound water (ω_b) is calculated by subtracting the amount of freezing water (ω_f) from the total water uptake (ω_t). Then, the bound water degree ($\chi = \omega_b/\omega_t$) is calculated from the ratio of the amount of bound water to the total water uptake.

Proton conductivity of the polymer membranes was measured by an ac impedance technique using an electrochemical impedance analyzer (CH Instrument model 604A), where the ac frequency was scanned from 100 kHz to 10 Hz at a voltage amplitude of 10 mV. Fully hydrated membranes were sandwiched into a Teflon conductivity cell equipped with Au plates. The temperature dependence of proton conductivity was carried out by controlling the temperature from 30 to 90 °C at 100% RH.

Methanol permeability of membranes was measured using a liquid permeation cell composed of two compartments, which were separated by a vertical membrane. The detailed description for estimating methanol permeability has been reported elsewhere [24]. The concentration of permeated methanol was analyzed on a gas chromatograph (VARIAN, 5200GC) equipped with 3-m capillary column packed with Polarpack Q (poly(ethylene glycol)-1000 supported on Shimalite F).

The cross-section morphology of the membranes was characterized by transmission electron microscopy (TEM) using JEOL JEM-1200CX-II microscope operating at 120 kV. The hybrid membranes were immersed in 1N Ag^+ aqueous solution overnight and rinsed with water for staining the hydrophilic domains. A 3 mm × 5 mm strip was cut from the membranes and was dried

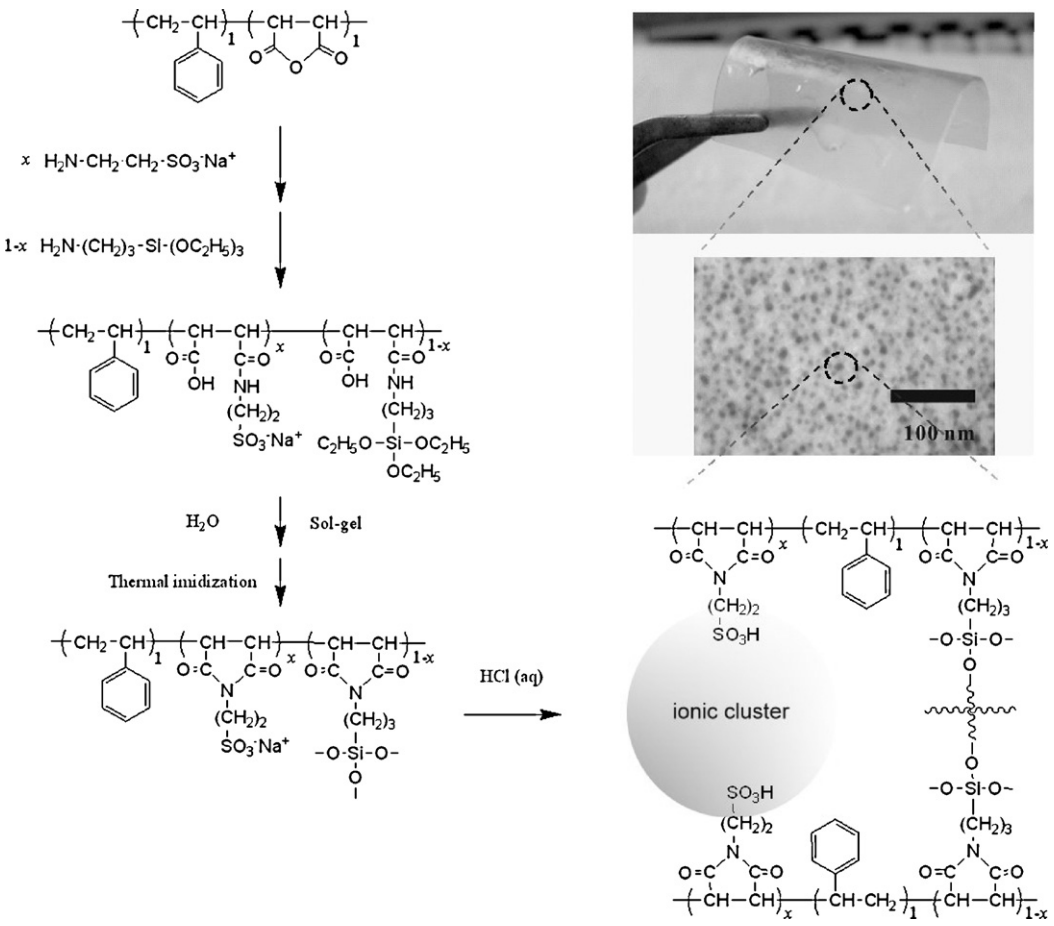

Scheme 1. Synthetic route and schematic representation for the cross-linked hydrocarbon ionomers.

under vacuum at 80 °C for 12 h. The sample was sectioned to yield 50 nm slices using an ultramicrotome. The slices were picked up with 200-mesh copper grids for TEM observation.

Single DMFC test was evaluated using a unit cell with an active area of 5 cm^2 fed with a 2.0 M methanol aqueous solution at the anode with a rate of 2 ml min^{-1} by a peristaltic micropump, and oxygen at the cathode with a rate of 100 ml min^{-1}. The membrane electrode assemblies for the single cell test were fabicated as follows. Catalyst ink was prepared by mixing catalyst powder (E-TEK 20% PtRu/XC-72 for anode and E-TEK Pt/XC-72 for cathode) with water (2 ml for 1 g of electrocatalyst), and then adding isopropanol (20 ml for 1 g of electrocatalyst) to avoid any ignition. 5% Nafion dispersion (Dupont) was added (0.8 g solid Nafion for 1 g of catalyst) to the catalyst slurry. Catalyst coating on gas diffusion layer (50 wt.% wet-proofing carbon paper, Toray) with 5 cm^2 active area was fabricated by brushing Pt/C catalyst ink. The catalyst loadings on the anode and cathode layers were both 2 mg Pt cm^{-2}. The catalyst-coated GDLs were hot-pressed with the hybrid membrane or Nafion-117 membrane (Du Pont) at 140 °CC under 30 kg cm^{-2} of pressure.

3. Results and discussion

3.1. Synthesis and characterization of the hybrid ionomer

The imidation of poly(maleic anhydride-co-styrene) with 2-aminoethanesulfonic acid sodium salt (AESA-Na) and aminopropyltriethoxysilane (APTES) proceeded quantitatively in DMSO to give the title ionomers (Scheme 1). A series of hybrid ionomers **A–D** with different side chain sulfonate groups (x) and APTES ($1-x$) were synthesized. The side chain composition was set at $x = 0.077–0.313$ by moles to obtain the ionomers with titrated ion exchange capacity (IEC) ranging from 0.28 to 1.10 mequiv. g^{-1} (Table 1). The molar ratio of siloxane to sulfonate group ($\alpha = (1-x)/x$) represented the cross-linking degree in the

Table 1
Compositions, water uptake, and methanol permeability of the hybrid ionomers.

Sample	x[a]	Cross-linking degree, α[b]	Water uptake (wt.%)	IEC (mequiv. g^{-1})	Methanol permeability, P (cm^2 s^{-1})	Breaking stress $\times 10^{-2}$ (Pa)
A	0.077	12.0	14.5	0.28	2.6×10^{-8}	14.5
B	0.199	4.0	21.4	0.71	7.9×10^{-8}	12.1
C	0.234	3.3	25.9	0.83	3.2×10^{-7}	10.2
D	0.313	2.2	39.5	1.10	7.8×10^{-7}	4.6
Nafion-117	–	–	24.3	0.91	2.5×10^{-6}	219.5

[a] x: repeat unit of pendent sulfonic acid group.
[b] α = –Si/–SO_3H = $(1-x)/x$.

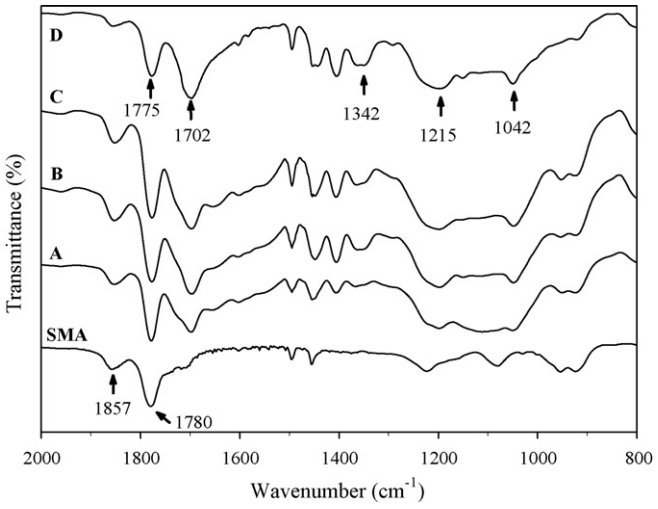

Fig. 1. FT-IR spectra of SMA and the hybrid ionomers.

membrane. Casting from DMSO solution of the ionomers gave a tough and flexible brown membrane with a thickness of 200 μm following a thermal imidation process at 200 °C under vacuum. The ionomers after thermal imidation would not dissolve in any polar aprotic solvent. These membranes were characterized by FT-IR, solid-state ^{13}C and ^{29}Si CP/MAS NMR.

The FT-IR spectra in the 800–2000 cm^{-1} region of the hybrid membranes and the raw poly are shown in Fig. 1. For poly(maleic anhydride-*co*-styrene), two absorption bands, at 1780 and 1857 cm^{-1}, show the valence oscillation of the cyclic anhydride structure. For the hybrid ionomers, the characteristic absorption bands at 1702, 1775 and 1342 cm^{-1}, being ascribed to symmetric and asymmetric imide carbonyl groups and the C–N–C absorption of the imide ring [26], respectively, with the absence of the cyclic anhydride peaks demonstrated the formation of imide structure and the success of the side chain reaction. The first noticeable difference among these membranes is the sharpening of the peaks at around 1042 and 1215 cm^{-1} which are assigned respectively to the $-SO_3^-$ symmetric and asymmetric stretching vibrations [27]. A progression in the relative intensity of these two bands toward a higher absorbance indicated an increasing concentration of a sulfonate group for membranes **A** to **D**.

Fig. 2 shows the ^{13}C CP/MAS NMR spectra of the membranes with different concentrations of sulfonate groups on side chain. The two peaks at $\delta = 10$ and 23 ppm are assigned to the methylene carbons in the α and β positions of the silicon atom, respectively. A broad signal, which ranged from 30 to 60 ppm, is composed of three superimposed peaks: the methylene carbon in the β and α positions at 36 and 52 ppm of the sulfonate group on the pendent AESA chain, and the methylene carbon on polymer backbone at $\delta = 42$ ppm. The other downfield peaks at $\delta = 128$ and 180 ppm are ascribed to the aromatic carbon atom and carbonyl carbon of imide ring [28].

Solid-state ^{29}Si NMR measurements were performed to gain further information regarding the structure of the inorganic side and to provide further information about the levels of condensation and the structure of the inorganic network of the hybrid materials. Fig. 3 shows the ^{29}Si CP/MAS NMR spectra of the samples which were prepared with different sulfonate contents, together with assignment to each T^1-, T^2- and T^3-group of silicon. These signals are attributed to condensed siloxane fragments in T^3 [$RSi(OSi)_3$] at $\delta = 65$ ppm, T^2 [$RSi(OR)(OSi)_2$] at $\delta = 55$ ppm and T^1 [$RSi(OR)_2(OSi)$] at $\delta = 47$ ppm arrangements, respectively [29,30]. The intensity of the T^3 resonance is found to be much higher than that of T^2 and T^1 in all samples, indicating a predominating degree of the three-dimensional silsesquioxane network in the hybrid membranes.

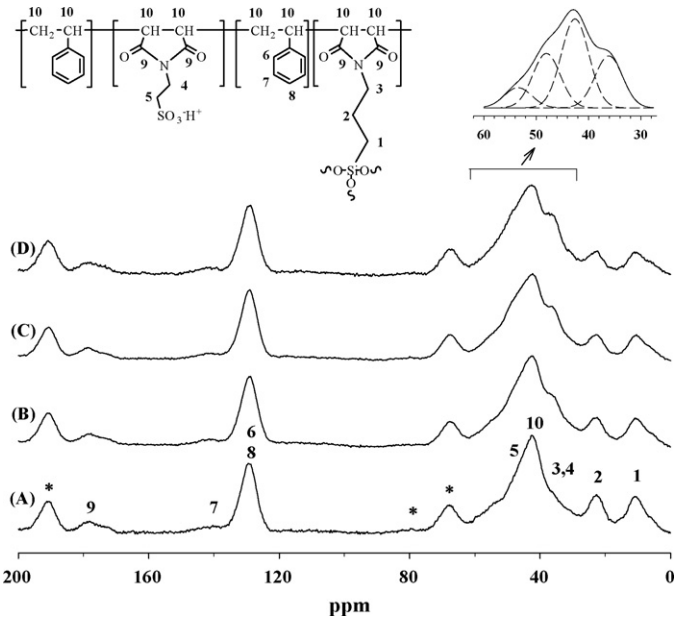

Fig. 2. ^{13}C CP/MAS NMR spectra of (A) membrane **A**, (B) membrane **B**, (C) membrane **C**, and (D) membrane **D**, respectively, together with the assignments of the peaks.

The aforementioned hybrid ionomers were subjected to differential scanning calorimeter (DSC) measurements to evaluate their thermal characteristics. The DSC thermograms of the cross-linked ionomers (Fig. 4a) showed a slight heat capacity change around 160–180 °C which corresponds to the glass transition temperature (T_g) of the motion of the poly(maleic imide-*co*-styrene) main chain, above which main chain motion takes place, as is usually observed for poly(maleic amide-*co*-styrene) [31]. It was observed that T_g decreased from 170 to 165 °C as ion exchange capacity increased. This indicates that the grafted sulfonic acid chain induces a relaxation process of the poly(maleic imide-*co*-styrene). This relaxation process may bring about a loose molecular packing which favors the adsorption of water between the polymer chains.

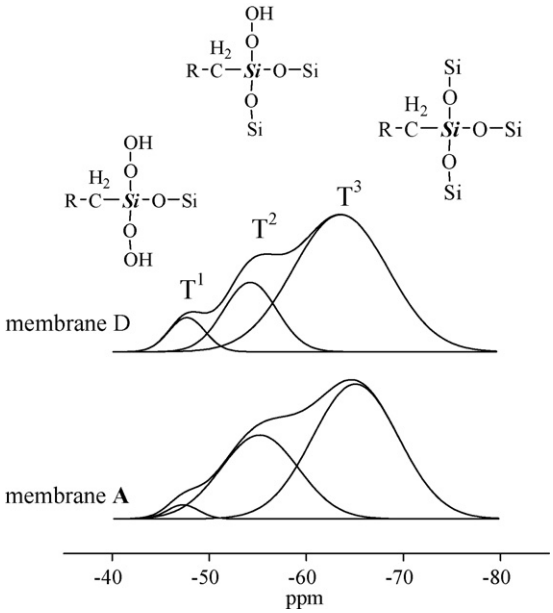

Fig. 3. ^{29}Si CP/MAS NMR spectra of the membrane **A** and membrane **D**.

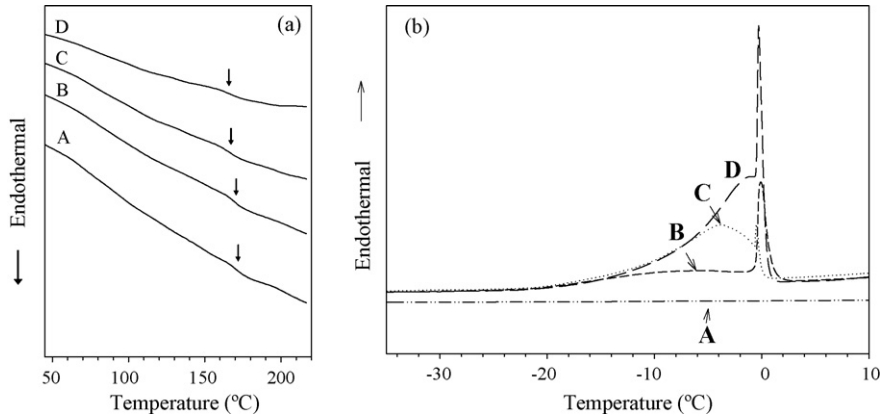

Fig. 4. (a) Comparison of the DSC curves over the temperature range 50–220 °C for the hybrid membranes and (b) DSC thermograms indicating the melting of water in the fully hydrated hybrid ionomers.

3.2. Swelling behavior and states of water

As a polymer electrolyte, the sulfonated poly(maleic imide-*co*-styrene) without being cross-linked by APTES showed considerable hydrophilicity. The chemical cross-linking of sulfonated poly(maleic imide-*co*-styrene) by APTES through the condensation of the silanol/silanol gave the ionomer good mechanical properties. The water uptake, expressed in grams of water adsorbed per gram of hydrated membrane, was evaluated as a measure of the degree of the swelling. As shown in Table 1, the water uptake increases from 14.5 to 39.5 wt.% as the IEC value raises from 0.28 to 1.1 mequiv. g^{-1}. These values correspond to 33.6, 21.3, 23.4, and 33.0 water molecules per sulfonic acid group (λ_t, Table 2) for membranes **A**–**D**, respectively. The dependence of λ_t on the cross-linking density, as shown in Fig. 4, exhibited an interesting funnel-like line. It is comprehensible that an increase of cross-linking density obstructs the adsorption of water. For membrane **A**, 33.6 of λ_t is a considerably high value, despite it having a high cross-linking degree (α = 12.0). This result evidenced that the hybrid membrane **A**, though featuring a much denser structure, consists of an interconnected porous network, while the inherent hydrophilic silicate sites in the hybrid matrix itself also serve as adsorbing sites for water.

The nature of water adsorption in proton conducting polymer membranes is of great importance. The states of water, such as free water and bound water in sulfonated polymers, directly affect the transportation of protons across the membranes. The association of water molecules with other species such as ionic and polar groups dominates the thermal transitions of water molecules. It has been shown that the bound water that forms a true solution with the polymer does not freeze at 0 °C, while the melting endotherm observed in a DSC thermogram at that temperature was due to the free and loosely bound water. The DSC thermograms of the fully hydrated hybrid membranes (Fig. 4b) showed that these samples, except membrane A, had a broad endothermic peak which consisted of two major melting peaks. The peaks corresponded to freezable water, including free water, at approximately 0 °C and loosely bound water at a range of −2 to −30 °C. The membranes with higher cross-linking degrees (α) apparently showed a lower melting point for water. As α increased to 12.0, i.e. membrane **A**, no endothermic peak was observed, indicating that the water molecules in membrane **A** are well bound by the highly cross-linked matrix.

The weight fractions of freezing water (ω_f) and bound water (ω_b) to the fully hydrated membranes and the bound water degrees were estimated by the melting enthalpy of endothermic peaks [32]. The percentage of the freezing water, as shown in Table 2, increased as the IEC value increased. This increasing free water percentage can be ascribed to the increasing hydrophilicity and decreasing cross-linking degree of the membranes. As α decreases, free water occupies the vacant space near the pendent sulfonate group and the loose polysiloxane network. The specific water molecules (free λ_f or bound λ_b) per sulfonic acid group were calculated from the specific water percentages divided by IEC values, as shown in Table 2. It has been known that the number of water molecules per sulfonic acid group correlates closely with the size of ionic clusters in ionomers [33]. Fig. 5a displays the dependence of λ_f and λ_b on cross-linking density. The reduced concentration of sulfonic acid groups, as well as the cross-linked siloxane framework occupying the space for free water, brought about the decreasing curve for λ_f. Furthermore, the similarity between the two curves of λ_b and λ_t suggested that bound water dominates the behavior of water adsorption in the hybrid membranes. The V-shaped curves of λ_b and λ_t are referred to as a compromise between the sulfonic group and siloxane matrix. At low cross-linking degrees (α = 2–4), the decrease in λ_b followed with the decrease in IEC values. At α = 12, sulfonic acid groups were confined in the robust polysiloxane network, and were expected to be incapable of binding with numerous water molecules; however, increasing siloxane segments encouraged a strong interaction between water and the well-established

Table 2
States of water for the hybrid ionomers.

Sample	T_{m_2} (°C)	Freezing water, ω_f (wt.%)	Bound water, ω_b (wt.%)	Bound water degree[a] (%)	λ_t[b]	λ_b[c]	λ_f[d]
A	–	0	14.5	100	33.6	33.6	0
B	−5.7	3.2	18.2	85.0	21.3	18.1	3.2
C	−3.8	6.0	19.9	88.4	23.4	18.0	5.4
D	−1.2	8.6	30.9	78.2	33.0	25.8	7.2
Nafion-117	−2.8	9.8	14.5	59.7	19.6	11.7	7.9

[a] ω_b/ω_t.
[b] λ_t = total H_2O/–SO_3H.
[c] λ_b = bound H_2O/–SO_3H.
[d] λ_f = free H_2O/–S.

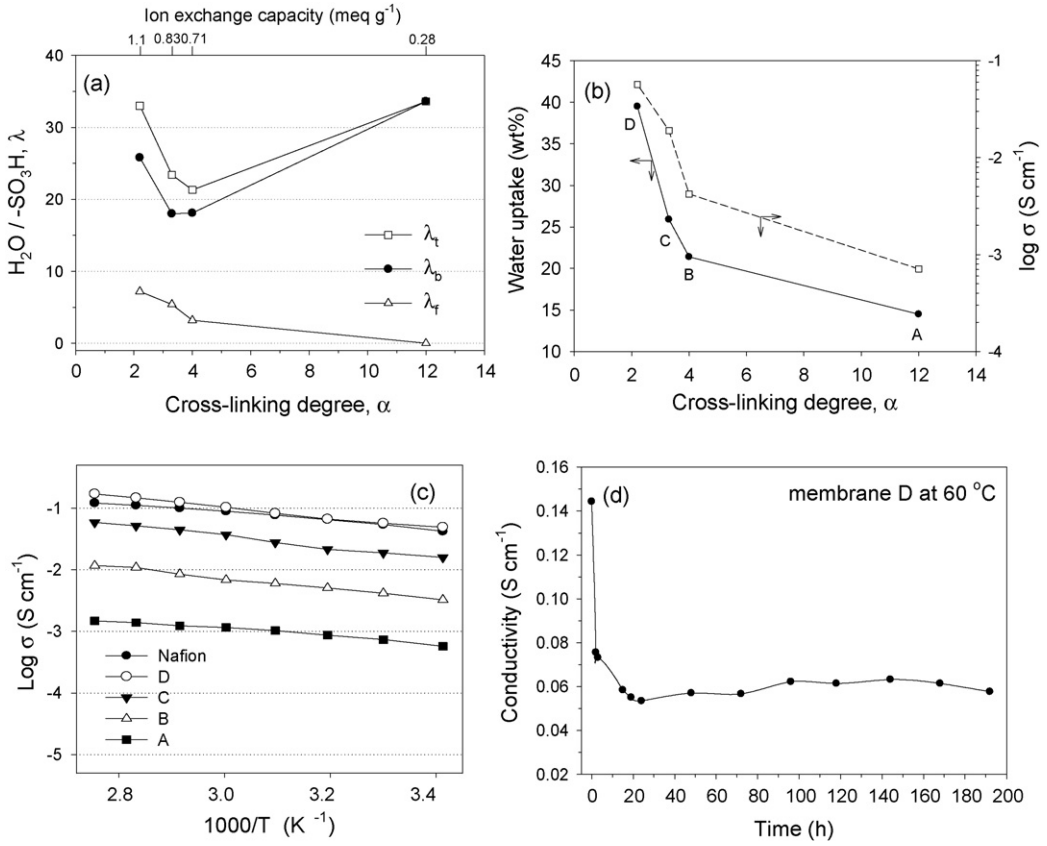

Fig. 5. (a) Specific water molecules per sulfonic acid group of hybrid membranes as a function of cross-linking degree, (b) dependence of water uptake and proton conductivity on cross-linking degrees, (c) Arrhenius plot of proton conductivity for Nafion-117 and the hybrid membranes at 100% RH and (d) time course of proton conductivity of membrane **D** at 60 °C and 100% RH.

polysiloxane framework by hydrogen bonding. Subsequently, this bonding led to an increase in λ_b. The specific interaction between water and the cross-linked polysiloxane network was characterized by the lower T_{m_2}, which appeared in DSC thermograms as reported previously [24]. In Table 2, the membranes **A**, **B** and **C** showed bound water degrees being higher than 85%. The bound water degree of membrane **D** is 78%, but even then it is still higher than Nafion-117 (60%). These results suggest significant phase-separated microstructures, as discussed below together with the results of TEM analyses.

3.3. Tensile strength

In this study, the breaking stress of the fully hydrated membrane was determined from the stress–strain curve measured at a strain rate of $8.3 \times 10^{-3}\ s^{-1}$. The data based on the average of five individual tensile tests are tabulated in Table 1. The breaking stress of Nafion-117 is also shown in Table 1 as a comparison. It is evident that the breaking stress is dependent on the cross-linking degree, and is reduced as the ion exchange capacity is increased. This can be related to the lower cross-linking degree and the higher water uptake of the membrane. The value of breaking stress is decreased from 1450 to 460 Pa, correspondingly.

3.4. Proton conductivity

The proton transfer behavior through the cross-linked hybrid membranes is envisaged as being essentially affected by the temperature, water uptake, IEC values and the cross-linking degree. The *in-plane* proton conductivity (σ) of the fully hydrated hybrid membranes (100% RH) is plotted as a function of temperature, as shown in Fig. 5c. The dependence of proton conductivity on temperature showed an Arrhenius relationship for all membranes. The **D** membrane showed the most preferable conductivity which is comparable to Nafion-117, and increased with rising temperatures to the order of $10^{-1}\ S\,cm^{-1}$ above 60 °C. Moreover, the slope in Fig. 5c is similar for the hybrid ionomers and Nafion-117, suggesting that these membranes have the same proton transfer kinetics involving Grötthus-type conduction. The conductivity measurement was carried out at 60 °C and 100% RH on a longer time scale (Fig. 5d). The **D** membrane showed a drop in proton conductivity within 20 h, but then kept a constant conductivity value of $0.06\ S\,cm^{-1}$ within acceptable error for 200 h, which confirms satisfactory hydrolytic stability [16,34].

The effect of the cross-linking degree on water uptake behavior and proton conductivity of the hybrid membranes is illustrated in Fig. 5b. Apparently, this system showed a similar decreasing trend both in conductivity and water uptake with an increasing cross-linking degree. The proton conductivity seemed to maintain at certain basic level around $10^{-3}\ S\,cm^{-1}$. This can be related to the transition between the water bound with $-SO_3H$ and the one associated with the polysiloxane framework. Here, the water bound with the polysiloxane framework played an important role in proton conductivity of the highly cross-linked membrane, i.e. membrane **A**. Since the IEC at high cross-linking degree was rather low, the main contribution towards proton conductivity would be from the bound water retained around the siloxane segment rather than from the water surrounding with sulfonic acid groups, as discussed in the water state section. This bound water-rich interconnected framework may accelerate proton transport by Grötthus-type conduction, as proven by the aforementioned low activation energy for proton conduction in Fig. 5c.

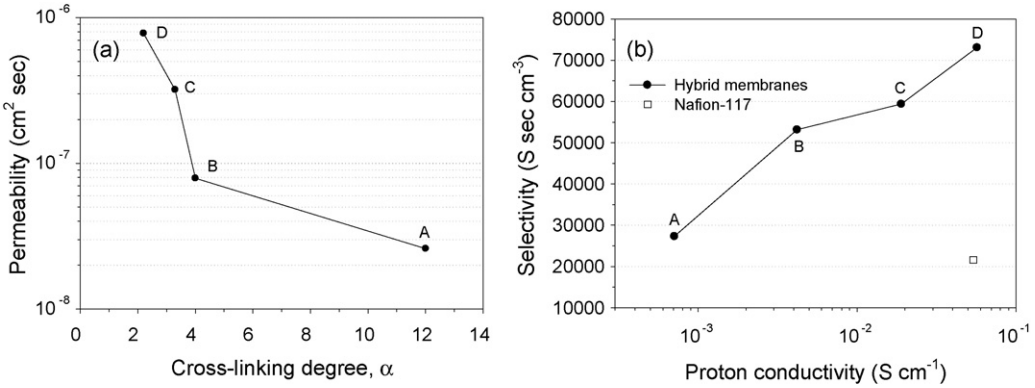

Fig. 6. (a) The dependence of methanol permeability at 30 °C on cross-linking degrees and (b) the performance trade-off plot of conductivity versus selectivity.

3.5. Methanol permeability

The methanol permeability of the hybrid ionomers was listed in Table 1. The methanol permeability of Nafion-117 is 2.5×10^{-6} cm^2 s^{-1}, which is consistent with the reported value of 2.3×10^{-6} cm^2 s^{-1} at 30 °C. In this study, a rather low permeability for the hybrid ionomers was obtained. The methanol permeability of **D** membrane is ~70% lower than that of Nafion-117, but had a higher water uptake and IEC. This suggests a strong blocking effect on methanol induced by the cross-linked network of polysiloxane. The influence of the cross-linking degree is illustrated by plotting the methanol permeability versus the α value. As depicted in Fig. 6a, the dependence of methanol permeability was similar to that of proton conductivity and water uptake. This indicates that the proton and methanol transport behaviors were highly related to the change of water uptake by the degree of cross-linking and the amount of bound water. However, it is not clear as to exactly why there is reduced permeability. Possible explanations would be a reduced concentration of methanol within the membrane, a lower methanol diffusion coefficient, or a combined reduction of both. Skou et al. [35] and Ren et al. [36] have reported that the concentration of methanol within Nafion pores is the same as that of the bulk solution. As shown by Easton et al., reduced crossover for Nafion/polypyrrole composite membranes is a result of decreased membrane porosity [37]. This is the behavior often observed for perfourosulfonate ionomers, due to the lack of the formation of hydrogen bonding for water as compared to the hydrocarbon-based ionomers. In the present study, membrane **D** with higher IEC showed a lower permeability than Nafion-117, of which water uptake is higher. High water uptake implies that the membrane has more vacant space for water to adsorb. It has been reported that the penetration of methanol across proton exchange membranes is strongly dependent on the water uptake; this is because the methanol permeates through the membranes as complex forms such as $CH_3OH_2^+$ and H_3O^+ [38]. Thus, it can be concluded that the specific interaction between water and the siloxane network, being evidenced by the melting behavior of water, reduces the water engaged with sulfonic acid groups and thus gradually decreases methanol permeability.

According to the above results of water uptake, state of water, the decrease in methanol permeability with increasing cross-linking degree, as seen in Fig. 6a, can be primarily attributed to the reduced porosity. The physical cross-linking of polysiloxane resulted in reduced porosity and induced a much denser structure to act as a methanol barrier.

In order to understand the performance trade-off between permeability and conductivity, we used the selectivity representing the transport characteristics of both the proton and methanol (σ/P) of the hybrid membranes and Nafion-117, as shown in Fig. 6b. Membrane **D** was 2.7 times more selective than membrane **A** and 3.3 times more selective than Nafion-117. Interestingly, the conductivity of the hybrid membranes did not decrease in order to gain its selectivity, as is normal behavior for proton exchange membranes [39–41], but instead increased. This unex-

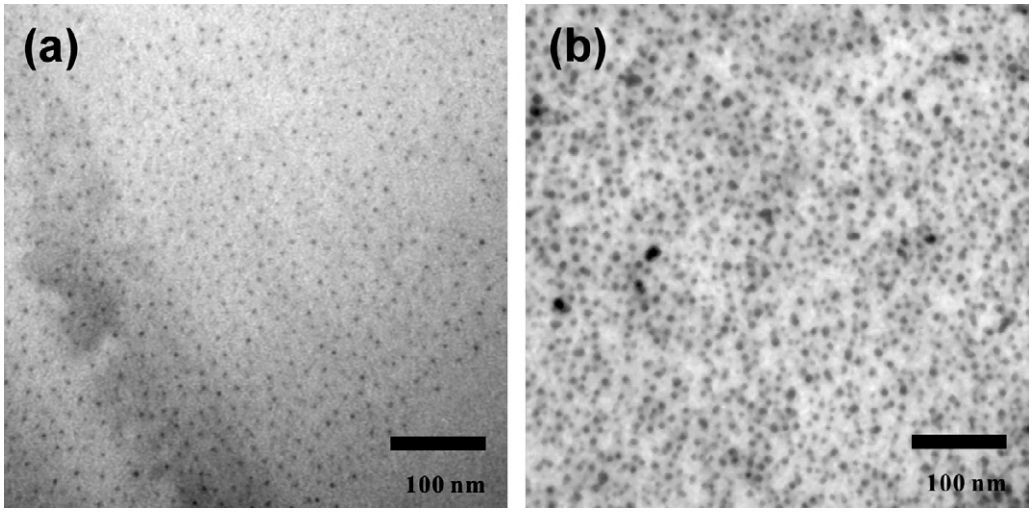

Fig. 7. TEM micrographs of (a) membrane **C** and (b) membrane **D** after stained with silver ions.

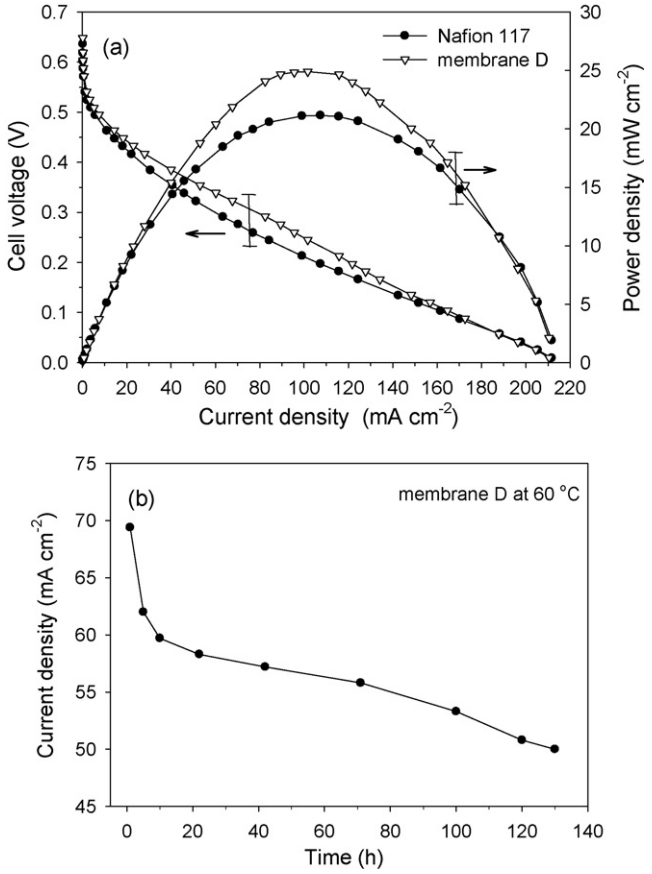

Fig. 8. Comparison of polarization curves for the single DMFC with membrane **D** and Nafion-117 as the electrolyte membrane (cell temperature: 60 °C; anode: 2 ml min^{-1} of 2.0 M methanol; cathode: O_2; flow rate: 100 ml min^{-1}; atmospheric pressure).

pected result is ascribed to the nature of poly(styrene-*co*-maleic imide). Poly(styrene-*co*-maleic anhydride) itself is known as a material with high affinity to alcohols due to its intermolecular hydrogen bonding [42]. This nature, together with the cross-linked network, bestowed membrane **D** with a low methanol permeability. As a result, the change in methanol permeability (by 30 times) was smaller than the improvement in proton conductivity (by 80 times) as the IEC changed from 0.28 to 1.1 mequiv. g^{-1}.

3.6. Microscopic observation

Transmission electron microscopy (TEM) analysis was performed on 50–80 nm thick slices of silver ion stained membranes. Fig. 7 shows the TEM results for membranes **B** and **D**. The dark regions represent localized hydrophilic domains, while the lighter regions represent hydrophobic domains. The micrographs provide direct evidence of a hydrophilic/hydrophobic microphase separation and spherical ionic clusters homogeneously distributed within the polymer, which are different from the archetypical proton conducting membrane, Nafion, in which a "cluster network" composed of 5–10 nm ionic clusters is interconnected by narrow ionic channels [24]. As is clearly seen in Fig. 7a, membrane **B** exhibited spherical ionic clusters with relatively uniform sizes of 2–3 nm. A similar microstructure has been reported for other categories of nonfluoro ionomers [41]. In the TEM image of membrane **D** (Fig. 7b), a large number of bigger ionic clusters (5–8 nm) was observed. The higher IEC causes the formation of such big clusters, which are larger than those of membrane **B**, and therefore, favors faster proton transportation. Furthermore, the poor connectivity between the spherical-shaped ionic clusters could be the reason for the attainment of the low methanol permeability. We suggest that the diffusion of the large complex formed by methanol and water is likely obstructed by the cross-linked polysiloxane network between the spherical ionic clusters; thus resulting in the high selectivity, as mentioned previously.

3.7. Single DMFC performance

The performance of the membrane electrode assemblies (MEAs) in the DMFC with membrane **D** and Nafion-117 as electrolyte membranes, E-TEK 20% Pt/XC-72 as cathode, and E-TEK 20% PtRu/XC-72 as anode, were evaluated in a single DMFC. The electrolyte membrane was sandwiched between the cathode and the anode by hot pressing. Membrane **D** exhibited a higher current density than Nafion-117 by 19 mA cm^{-2} in the ohmic resistance region (0.29 V), as shown in the polarization curves of Fig. 8a. The corresponding power density curves of these MEAs are also displayed in Fig. 8b. Membrane **D** showed a good power density of 25.0 mW cm^{-2}, which is better than that of Nafion-117.

4. Conclusion

Proton conducting hydrocarbon ionomers, manifested as sulfonated poly(maleic imide-*co*-styrene), were synthesized. Covalently cross-linked polysiloxane/poly(maleic imide-*co*-styrene) hybrid membranes showed good proton conductivities comparable to Nafion. The methanol permeating behavior was found to depend on the cross-linking degree and the hydrogen bonding between water molecules and the polysiloxane networks. The state of water, as indicated by thermal transitions, can be directly connected to the resulting properties of respective membranes. By combining the microstructure observations, proton conduction and the methanol permeation results, it can be concluded that the incorporation of polysiloxane framework in sulfonated poly(maleic imide-*co*-styrene) induced a significant reduction in the ionic cluster size. The well-distributed spherical ionic clusters effectively block the permeation of methanol. The resultant methanol permeability was more than 1 order of magnitude lower than Nafion-117.

Acknowledgments

The authors gratefully acknowledge the National Science Council, Taipei, Taiwan for their generous financial support of this research.

References

[1] W. Vielstich, A. Lamm, H. Gasteiger, Handbook of Fuel-Cells: Fundamentals, Technology, Application, Wiley, New York, 2004.
[2] R.F. Service, Science 315 (2009) 172.
[3] L. Carrette, K.A. Friedrich, U. Stimming, Fuel Cells 1 (2001) 5–39.
[4] M. Winter, R. Brodd, J. Chem. Rev. 104 (2004) 4245–4269.
[5] O. Diat, G. Gebel, Nat. Mater. 7 (2008) 13–14.
[6] K. Schmidt-Rohr, Q. Chen, Nat. Mater. 7 (2008) 75–83.
[7] K.A. Mauritz, R.B. Moore, Chem. Rev. 104 (2004) 4535–4585.
[8] Y. Yang, S. Holdcroft, Fuel Cells 5 (2005) 171–186.
[9] J.A. Kerres, Fuel Cells 5 (2005) 230–247.
[10] K.D. Kreuer, Chem. Mater. 8 (1996) 610–641.
[11] Q. Li, R. He, J.O. Jensen, N. Bjerrum, J. Chem. Mater. 15 (2003) 4896–4915.
[12] C. Manea, M. Mulder, J. Membr. Sci. 206 (2002) 443.
[13] J.S. Park, J.W. Park, E. Ruckenstein, Polymer 42 (2001) 4271–4280.
[14] S. Tan, J.H. Tieu, D. Bélanger, J. Phys. Chem. B 109 (2005) 14085–14092.
[15] J. Kerres, C.M. Tang, C. Graf, Ind. Eng. Chem. Res. 43 (2004) 4571–4579.
[16] C.H. Lee, H.B. Park, Y.S. Chung, Y.M. Lee, B.D. Freeman, Macromolecules 39 (2006) 755–764.
[17] Kerres, J. Fuel Cells 6 (2006) 251–260.
[18] Y. Chikashige, Y. Chikyu, K. Miyatake, M. Watanabe, Macromol. Chem. Phys. 207 (2006) 1334–1343.
[19] Q. Li, C. Pan, J.O. Jensen, P. Noy, N. Bjerrum, J. Chem. Mater. 19 (2007) 350–352.
[20] W.J. Liang, P.L. Kuo, Macromolecules 37 (2004) 840–845.

[21] W.J. Liang, Y.P. Chen, C.P. Wu, P.L. Kuo, J. Phys. Chem. B 109 (2005) 24311–24318.
[22] W.J. Liang, C.P. Wu, C.Y. Hsu, P.L. Kuo, J. Polym. Sci. Part A: Polym. Chem. 44 (2006) 3444–3453.
[23] P.L. Kuo, W.F. Chen, W.J. Liang, J. Polym. Sci. Part A: Polym. Chem. 43 (2005) 3359–3367.
[24] W.F. Chen, P.L. Kuo, Macromolecules 40 (2007) 1987–1994.
[25] W.F. Chen, J.S. Wu, P.L. Kuo, Chem. Mater. 20 (2008) 5756–5767.
[26] D. Jamróz, Y. Maréchal, J. Phys. Chem. B 109 (2005) 19664–19675.
[27] T. Yasuda, Y. Li, K. Miyatake, M. Hirai, M. Nanasawa, M. Watanabe, J. Polym. Sci. Part A: Polym. Chem. 44 (2006) 3995–4005.
[28] P.P. Chu, J.M. Huang, H.D. Wu, C.R. Chiang, F.C. Chang, J. Polym. Sci. Part B: Polym. Phys. 37 (1999) 1155–1163.
[29] W.J. Liang, P.L. Kuo, J. Polym. Sci. Part A: Polym. Chem. 42 (2004) 151–161.
[30] V. Monteil, J. Stumbaum, R. Thomann, S. Mecking, Macromolecules 39 (2006) 2056–2062.
[31] H. Yan, X. Zhu, J. Appl. Polym. Sci. 74 (1999) 97–105.
[32] Y.S. Kim, L. Dong, M.A. Hickner, T.E. Glass, V. Webb, J.E. McGrath, Macromolecules 36 (2003) 6281.
[33] W.L. Harrison, M.A. Hickner, Y.S. Kim, J.E. McGrath, Fuel Cells 5 (2005) 201–212.
[34] N. Asano, K. Miyatake, M. Watanabe, Chem Mater. 16 (2004) 2841–2843.
[35] E. Skou, P. Kauranen, J. Hentschel, Solid State Ionics 97 (1997) 333–337.
[36] X. Ren, T.E. Springer, T.A. Zawodzinski, S. Gottesfeld, J. Electrochem. Soc. 147 (2000) 466–474.
[37] E.B. Easton, B.L. Langsdorf, J.A. Hughes, J. Sultan, Z. Qi, A. Kaufman, P.G. Pickup, J. Electrochem. Soc. 150 (2003) C735–C739.
[38] J.O. Won, H.H. Park, Y.J. Kim, S.W. Choi, H.Y. Ha, I.H. Oh, H.S. Kim, Y.S. Kang, K. Ihn, J. Macromol. 36 (2003) 3228–3234.
[39] D.S. Kim, G.P. Robertson, Y.S. Kim, M.D. Guiver, Macromolecules 42 (2009) 957–963.
[40] Y.A. Elabd, E. Napadensky, C.W. Walker, K.I. Winey, Macromolecules 39 (2006) 399–407.
[41] M.M. Hasani-Sadrabadi, E. Dashtimoghadam, F.S. Majedi, K. Kabiri, J. Power Sources 190 (2009) 318–321.
[42] Y.G. Devrim, Z. Rzaev, E. Pişkin, Macromol. Chem. Phys. 208 (2007) 175–187.